On the Use of Regularization Techniques in Numerical Inverse-Scattering Solutions for Microwave Imaging Applications

Salvatore Caorsi, Stefano Ciaramella, Gian Luigi Gragnani, *Member, IEEE,* and Matteo Pastorino, *Member, IEEE*

Abstract— **This paper deals with integral-equation-based numerical methods for microwave imaging using regularization procedures to overcome ill-conditioning problems. The strong dependence of reconstruction quality on "a priori" information is discussed. Such information is required to select a suitable number of independent columns when using truncated pseudoinversions (or other regularization parameters, in different cases) for accurate dielectric reconstructions. Moreover, a criterion for the choice of the optimal number of independent columns is proposed, and the possibility of making this choice less critical by using a multiview version of the method is explored. Finally, a modified procedure is presented that further increases the range from which to choose the number of independent columns that allows one to achieve acceptable reconstructions.**

I. Introduction

THE PROBLEM of reconstructing dielectric objects by using interrogating microwave and near-field scattering data has been widely considered in recent years, and many papers have been published on this subject. Algorithmic aspects constitute the chief obstacle to the development of efficient and practical reconstruction systems. In the past, promising results were obtained by methods based on diffraction tomography [1], [2]; such methods related the dielectric parameters of unknown configurations to scattering data via Fourier transforms. Recently, several limitations of these methods were pointed out [3], [4], and some interesting approaches were proposed that make use of numerical methods (especially the moment method (MoM) [5]) in order to obtain approximate solutions to the integral equations of the inverse scattering problem [6]–[9]. In most of these approaches, the problem solution is reduced to the solution of linear systems of algebraic equations. Unfortunately, the ill-posedness of the analytical problem is reflected in the ill-conditioning of the discretized problem. Usually, a regularization procedure is required to obtain a well-behaved problem solution, that is an acceptable approximation for the solution of the original ill-conditioned problem [10], [11]. When an inverse problem is expressed in discretized form, the use of a regularization procedure is usually a well-conditioned way of solving a set of linear equations. Among others, the most widely used regularization procedures are truncated pseudoinversion [12], [13] (used, for example, in [8], [14], [15]), singular-value decomposition [16] (used in [17], [18]), and Tikhonov regularization [19] (used in [20], [21]). Other references can be found in all such papers. It should be noted that one of the most important (but not completely solved) problems involved in inverse-scattering methods is represented by the nonuniqueness issue. This crucial point is not addressed in this work, so we refer the reader to [22], [23] and to the many references cited therein.

The objective of the present paper is threefold. First, we start with some considerations about the application of regularization procedures in dealing with inverse problems related to microwave imaging. In particular, we aim to stress that great care must be exercised in evaluating numerical simulation results, as regularization parameters (which have usually to be selected for any regularization procedure) may strongly depend on the problem configuration considered. As a consequence, results may be significantly dependent on *a priori* knowledge. If one provides numerical results without specifying the fixed regularization parameters, one runs the risk of furnishing results unhelpful for a further insight into dielectric reconstruction methodologies.

The second objective (resulting from the above considerations) is to propose a suitable criterion for the choice of the optimal regularization parameters for 3D and 2D numerical solutions to the inverse-scattering problem. We consider the application of a truncated pseudoinversion previously used by us, that is, a regularization procedure that minimizes both the residual of the system obtained by the MoM and the norm of the solution. However, the considerations reported can be adapted to the applications of approaches based on other regularization algorithms. Our result are compared with those yielded by the criterion suggested by Ney *et al.* [8], which, to the best of our knowledge, is the only criterion so far proposed (and probably used) for microwave imaging purposes.

Finally, a modified numerical method is presented that seems able to improve the accuracy of current moment-method-based approaches to microwave imaging [14]. The method is based on the association of the electric field integral equation (EFIE) for the direct scattering problem with the Fredholm integral equation for the inverse scattering problem. The approach does not require a significant increase in the computational load, and keeps some interesting features of the integral-equation-based numerical solution described in Section II.

In the following, we outline the mathematical formulation of the integral-equation numerical solution and discuss the

Manuscript received August 7, 1992; revised June 23, 1994.

The authors are with the Department of Biophysical and Electronic Engineering, University of Genoa, 16145 Genoa, Italy.

IEEE Log Number 9407468.

above topics on the basis of several numerical examples. All the mathematical aspects and the numerical results are related to three-dimensional configurations only, except for the discussion on the application of multiview techniques (basic to obtaining realistic reconstructions), which concern a two-dimensional geometry. At present, multiview approaches in three-dimensional form are not available.

II. Moment-Method Solution to Inverse Scattering

In this section, we briefly outline the mathematical formulation for a 3D configuration. With reference to Fig. 1, we consider a fixed investigation domain, V, and an observation domain, D. V' is the domain of an object whose location (inside V), surface shape, and complex dielectric permittivity distribution ($\varepsilon^*(\boldsymbol{r})$) are unknown. We assume a homogeneous propagation medium (ε_p^*) and the time-dependence of $\exp(j\omega t)$. If $\boldsymbol{E}_{\text{inc}}(\boldsymbol{r})$ is a known incident electric field and $\boldsymbol{E}_{\text{tot}}(\boldsymbol{r})$ is measured inside D, the following integral equation can be derived, in compliance with Sommerfeld's radiation condition, under e.m. decoupling assumptions [24], [25]:

$$\int_v \boldsymbol{K}(\boldsymbol{r}') \cdot \Gamma_0(\boldsymbol{r}, \boldsymbol{r}') d\boldsymbol{r}' = \boldsymbol{E}_{\text{tot}}(\boldsymbol{r}) - \boldsymbol{E}_{\text{inc}}(\boldsymbol{r}) \qquad \boldsymbol{r} \in D \quad (1)$$

where $\boldsymbol{K}(\boldsymbol{r})$ is the volume equivalent current density, which can be expressed as

$$\boldsymbol{K}(\boldsymbol{r}) = V(\boldsymbol{r}) \boldsymbol{E}_{\text{tot}}(\boldsymbol{r}) \qquad \boldsymbol{r} \in d \quad (2)$$

and $V(\boldsymbol{r})$ is the *scattering potential* given by $V(\boldsymbol{r}) = j\omega(\varepsilon^*(\boldsymbol{r}) - \varepsilon_p^*)$. In relation (1), $\Gamma_0(\boldsymbol{r}, \boldsymbol{r}')$ is the dyadic Green function for free space [25]. Usually, this relation is evaluated for a fixed number M of measurements points. Application of the MoM to (1) leads to the following system to be inverted [5], [6]:

$$\Gamma_{\text{MXN}} \underline{K}_{\text{NX1}} = \underline{E}^t_{\text{MX1}} - \underline{E}^i_{\text{MX1}}. \quad (3)$$

Due to ill-conditioning, system (3) is not inverted directly, and estimated solutions obtained by means of regularization procedures are utilized. The estimated $\underline{K}_{\text{NX1}}$ is used to compute the total electric field inside V' by

$$\boldsymbol{E}_{\text{tot}}(\boldsymbol{r}) = \boldsymbol{E}_{\text{inc}}(\boldsymbol{r}) + \sum_{n=1}^{N} \boldsymbol{K}_n \cdot \int_{V_n} f_n(\boldsymbol{r}'_n) \Gamma_0(\boldsymbol{r}, \boldsymbol{r}'_n) d\boldsymbol{r}'_n \qquad \boldsymbol{r} \in V \quad (4)$$

where $\boldsymbol{K}_n f_n(\boldsymbol{r}'_n)$ are the nth terms in the expansion used for $\boldsymbol{K}(\boldsymbol{r})$ in the application of the MoM to (1) ($f_n(\boldsymbol{r}'_n) = 1$, if $\boldsymbol{r}' \in V_n$, and $f_n(\boldsymbol{r}'_n) = 0$, otherwise) and V_n denotes the domain of the function $f_n(\boldsymbol{r}'_n)$. Once $\boldsymbol{E}_{\text{tot}}(\boldsymbol{r}), \boldsymbol{r} \in V$ is known (in an approximate way, by relation (4)), we derive the approximate distribution of dielectric parameters from the relation defining the equivalent current density $\boldsymbol{K}(\boldsymbol{r})$ (2). It is worth noting that the original scheme of the approach has been modified in several papers in order to extend the application range, or to improve the capabilities of the method. For example, the approach was made linear by using the classical Born approximation in [26]. A multiview version was used in [27], [14], and iterative schemes were derived in [20].

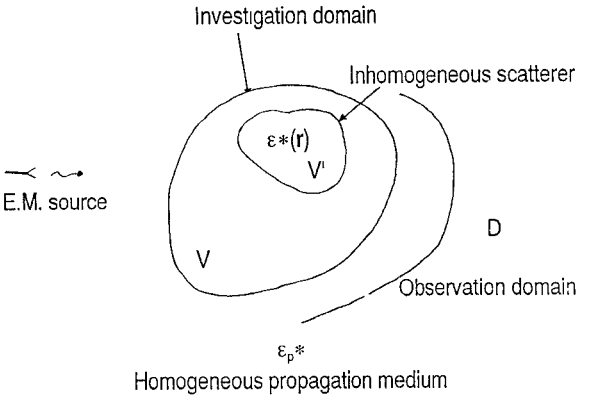

Fig. 1. Problem geometry.

III. Discussion and Results

Let us consider, for the sake of illustration, the same example of 3D reconstruction as given in [20] (and there used for a comparison with [28], even though the examples described in [28] were quite different). A cubical investigation domain (side $\lambda_n \times \lambda_n \times \lambda_n$) is illuminated by a unit plane wave polarized with the electric field in the z direction and propagating along the x axis. The domain is partitioned into 27 equal subdomains, and a homogeneous lossless scatterer ($\varepsilon_r = 3.0$) occupies a whole subdomain. Moreover, 27 measurement points are arranged as shown in Fig. 2. Starting from the synthetic data obtained by solving the direct scattering problem numerically, and subsequently affected by uniform errors [28], the inversion procedure described in Section II is applied to reconstruct the object.

The pseudoinversion algorithm applied to system (3) generates an estimate $\underline{K}_{\text{NX1}}$ such that the norm of the residual produced by this estimate is minimum, within the constraint that the norm of the estimate be minimum [12], [11]. In other words, this algorithm provides the simultaneous minimizations of the following norms: $\|\Gamma_{\text{MXN}} \underline{K}_{\text{NX1}} - (\underline{E}^t_{\text{MX1}} - \underline{E}^i_{\text{MX1}})\|$ and $\|\underline{K}_{\text{NX1}}\|$. In order to obtain the pseudoinverse solution of (3), one has to fix the number of columns of the Green matrix considered linearly independent. This is required by the Gram-Schmidt orthogonalization procedure used for the pseudoinversion [12]. However, it is well known that each regularization method requires that a critical parameter be fixed, whose *optimal* value "is crucial to the amenability and numerical implementation of the method" [11]. It is also worth noting that the pseudoinversion algorithm seems to behave not very differently from filtered singular-value decomposition, which is another suitable technique for regularizing problems of this kind.

For the considered example, Fig. 3 gives the reconstructed values of the scatterer's dielectric permittivity. As can be seen, the reconstruction quality depends on the number of independent columns chosen. Indeed, all values, from the background value to values of the order of some hundreds, can be obtained (including the exact value).

This example demonstrates that providing results without specifying the regularization parameters used is meaningless, and that the reconstruction quality is strictly related to the *a*

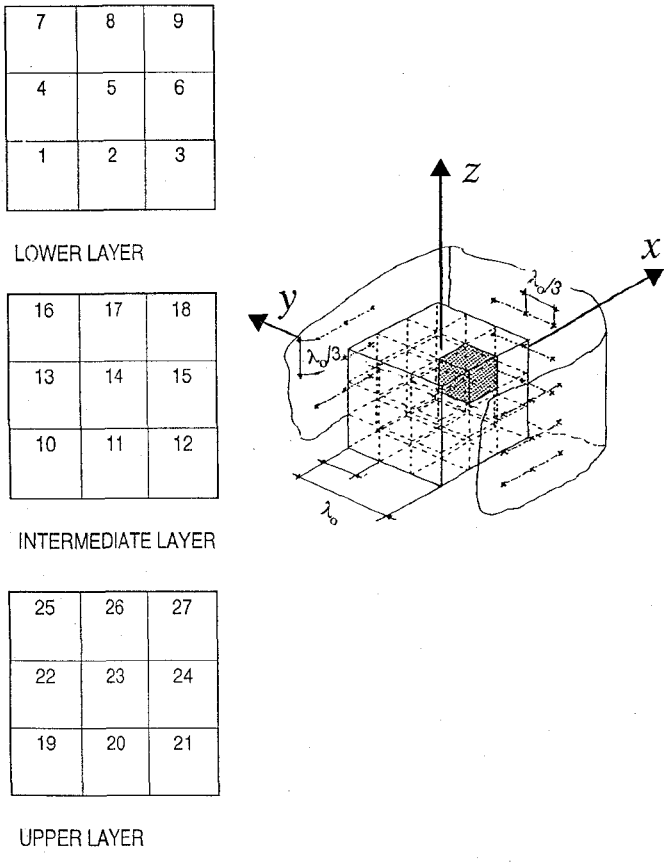

Fig. 2. Geometrical configuration for the 3D numerical example.

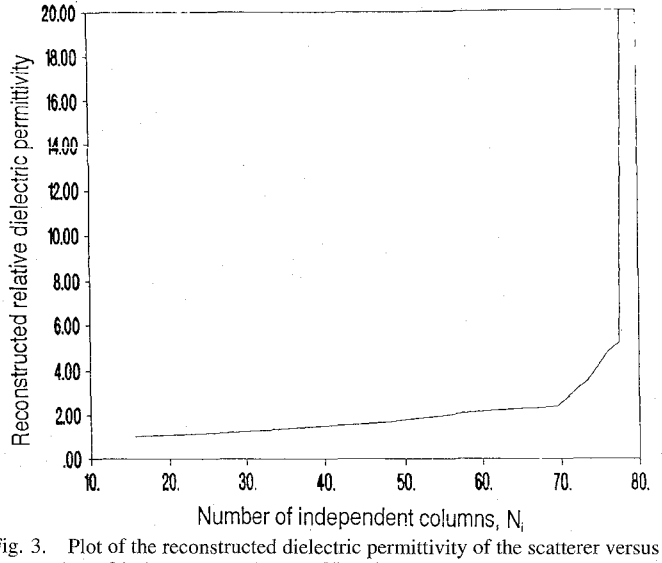

Fig. 3. Plot of the reconstructed dielectric permittivity of the scatterer versus the number of independent columns (N_i) of the Breen matrix.

priori information that must be used to fix these parameters. Moreover, the reconstruction quality of the background must be assessed.

Fig. 4 shows the plots of the parameters β_1 and β_2, defined as:

$$\beta_1 = \frac{|\varepsilon_r(k) - \underline{\varepsilon}(k)|}{\varepsilon_r(k)} \tag{5}$$

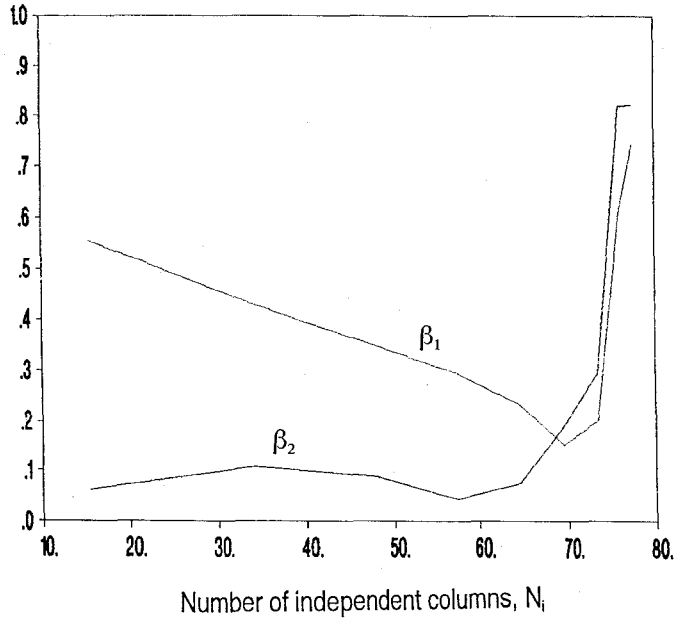

Fig. 4. Parameters β_1 and β_2 against the number of independent columns (N_i).

$$\beta_2 = \max_{i \neq k} \frac{|\varepsilon_r(i) - 1|}{\varepsilon_r(k)} \tag{6}$$

where $\varepsilon_r(i)$ and $\underline{\varepsilon}(i)$ stand for the original and reconstructed relative dielectric permittivities in the ith cell. The scatterer is contained in the kth cell (referring to Fig. 2, $k = 22$). According to relations (5) and (6), β_1 is a percentage error on the reconstruction of the scatterer's dielectric permittivity, and β_2 refers to the empty cells. A perfect reconstruction would yield $\beta_1 = \beta_2 = 0$. In particular, Fig. 4 points out that the behaviors of the two parameters against the number of independent columns are different; this typical situation occurred in almost all the simulations performed. As can be noticed, the best reconstruction of the scatterer's dielectric permittivity is obtained for a number of independent columns different from the one related to the best reconstruction of the background. Moreover, when the reconstruction of the scatterer is very accurate, large errors affect the reconstruction of the background.

The above considerations point out the need for a criterion to choose the number of independent columns for the pseudoinversion algorithm. As far as we know, the only criterion so far proposed (and perhaps used) is the one suggested in [8]. It was derived from the reconstruction of a one-dimensional structure, but the authors stated that the conclusions drawn in this case applied to all the configurations considered by them. The Ney-Smith-Stuchly Criterion (NSSC) is based on the plot of the norm of the reconstructed equivalent current density normalized to the norm of the original current density; the optimal number of independent columns has to be selected "just before" this quantity begins to increase significantly.

In our simulations, we used the following criterion: we consider the behaviors of the norms of the reconstructed equivalent current densities (or of the dielectric permittivities) inside the scatterer and in the background medium, and the optimal value to be selected corresponds to the intersection of

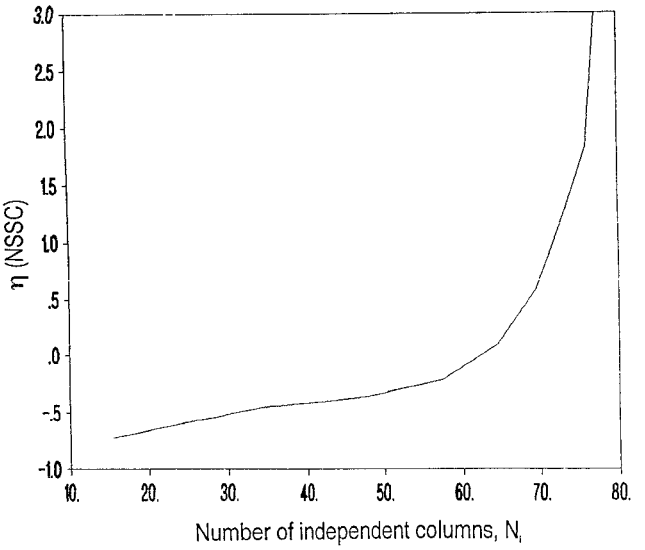

Fig. 5. Parameter η (used for the NSSC) against the number of independent columns (N_i).

the two plots. For comparison, Fig. 5 gives the behavior of the parameter η, which is defined as follows:

$$\eta = \log \frac{\|\underline{K}_{\mathrm{NX1}}\|}{\|\underline{K}_{\mathrm{NX1(original)}}\|} \tag{7}$$

where $\|\underline{K}_{\mathrm{NX1}}\|$ and $\|\underline{K}_{\mathrm{NX1(original)}}\|$ stand for the norms of the array obtained by solving system (4) and of the original array, respectively. The parameter η represents the normalized norm of the solution, as required by the NSSC. Table I gives the reconstructed values of the relative dielectric permittivities inside the 27 cells of the investigation domain; they were obtained by following the two criteria (for the NSSC, we fixed $N_i = 48$, $N_i = 57$, $N_i = 64$ and $N_i = 72$). As can be seen, the results are not very different. For the proposed criterion, the number to be used is unequivocally defined, whereas, for the NSSC, the value "just before beginning" can be chosen from a range of numbers, which result in different reconstructions (in some cases, affected by significant errors).

However, the new criterion requires one to know exactly which are the full and the empty cells, while the NSSC requires one to know the norm of the reconstructed equivalent current density in the whole domain and the norm of the unknown original equivalent current density, even if the latter is a constant quantity. On the other hand, it is evident that both criteria cannot be used for an on-line selection of columns, since the computation of the pseudoinverse matrix for all N_i values for any reconstruction is impractical. In addition, the possibility of computing the pseudoinverse matrix off line, once and for all, is one of the most important features of integral-equation-based microwave imaging approaches, as it allows one to develop more efficient multiview versions [14]. As a consequence, the optimal number of independent columns should be selected "a priori" in order to fix adequate operating conditions (suitable investigation and observation domains, numbers and kinds of testing and expansion functions, frequency, etc.) on the basis of "a priori" information about the nature of the scatterer under test (i.e., dimensions,

TABLE I
RECONSTRUCTED VALUES OF THE RELATIVE DIELECTRIC PERMITTIVITY INSIDE THE SCATTERER BY USING THE CRITERIA

	CCGPC		NSSC (in [8])		
Cell number	$N_i = 69$	$N_i = 57$	$N_i = 48$	$N_i = 64$	$N_i = 72$
1	1.12	1.08	0.99	1.22	0.91
2	0.96	1.10	1.03	1.12	0.88
3	0.76	1.02	1.11	1.06	0.64
4	0.91	0.97	1.07	0.89	1.36
5	1.07	1.01	1.04	1.16	0.94
6	1.31	1.13	1.07	1.22	1.32
7	0.86	1.00	0.98	1.07	0.58
8	0.99	1.04	1.06	0.97	1.16
9	0.84	0.95	0.99	0.83	0.71
10	0.93	1.03	0.97	0.99	1.02
11	0.69	1.02	1.11	0.90	1.14
12	0.95	0.84	0.87	0.90	1.01
13	0.80	1.11	1.26	0.88	0.73
14	0.95	1.12	0.97	1.03	1.39
15	0.86	0.94	0 90	0.79	0.30
16	0.96	0.92	0.88	0.87	0.27
17	1.37	0.97	0.96	1.07	1.18
18	1.04	0.96	0.99	0.90	1.04
19	1.10	1.04	0.107	1.03	0.78
20	0.96	1.02	0.105	1.01	0.95
21	0.98	1.07	0.106	0.99	1.04
22	2.54	2.11	1.96	2.30	3.61
23	1.00	1.03	0.98	0.97	1.19
24	1.03	0.92	1.02	0.94	1.34
25	1.07	0.99	1.04	1.05	1.12
26	1.08	1.05	1.07	1.20	0.81
27	1.04	1.07	1.04	1 10	1.01

ranges of dielectric permittivities and electric conductivities, noise levels, etc.). In other words, one should know "a priori" what class of scatterers can be successfully reconstructed (with an optimal or suboptimal quality) for a fixed number of independent columns. In the simulations required to obtain this information, the location of a testing scatterer is assumed to be known.

However, a severe limitation appears evident from Figs. 4 and 5. A small error in choosing the *optimal* number of independent columns (whichever criterion is used) will result in a large error on the dielectric reconstruction, due to the ill-conditioning of the inverse-scattering formulation considered. For example, if we assume $N_i = 40$, the error on the reconstruction of the scatterer becomes 40%, and the background is affected by a maximum error of about 10%. This fact points out that the class of scatterers that can be successfully reconstructed for a given configuration is very limited.

As another example, we considered a more complex scattering object, made up of two concentric spheres with different dielectric permittivities. We assumed the same geometrical configuration as shown in Fig. 2, but, in this case, we considered an investigation domain of dimensions $4/3\lambda_n \times 4/3\lambda_n \times 4/3\lambda_n$, partitioned into 64 discretization cells. The two spheres were centered at point $(\lambda_n/6, -\lambda_n/6, -\lambda_n/6)$. The radii of the two spheres were $a = \lambda_x/6$ and $b = \lambda_n/2$. The original relative dielectric permittivities were equal to 2.5 for the inner sphere and 1.5 for the outer one. The scattered-field data inside the measurement domain were computed by using the Mie series

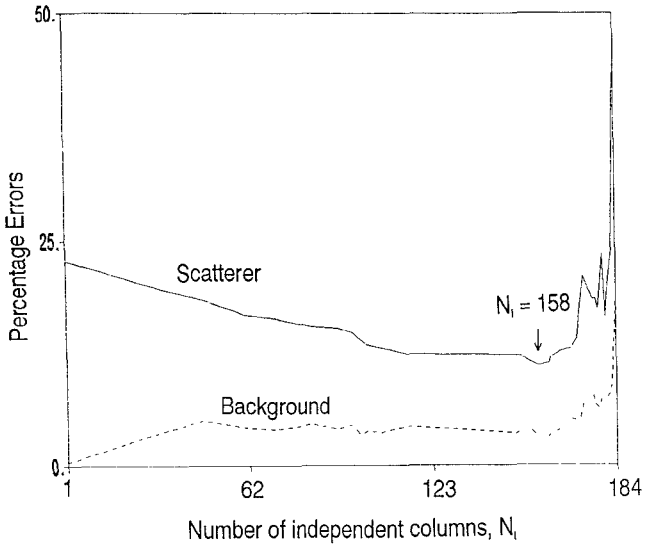

Fig. 6. Percentage errors on the reconstructions of the relative dielectric permittivities inside the two concentric spheres (continuous line) and in the background (dashed line).

solution [29]. Fig. 6 gives the results of the reconstruction process: in particular, the continuous line indicates the mean relative errors inside the scatterer (these errors are a generalization of the parameter β_1, that is, the mean values assumed by the parameter β_1 in all the discretization cells containing at least a part of the scatterer); the dashed line indicates the percentage errors on the reconstructed relative dielectric permittivity in the background (mean values computed for all the empty cells). For each discretization cell, the actual permittivity value was assumed to be equal to the value obtained by weighting the cell portions occupied by the two spheres with the permittivity values of the spheres. In this case, as can be noticed, the two plots do not overlap, and the relative errors on the reconstruction of the scatterer are always greater than twice the errors on the reconstruction of the background. Of course, the most acceptable reconstruction is achieved for $N_i = 158$. For this value of N_i, we reached the following percentage errors inside the full cells: maximum error, 31.0%; mean error, 11.4%; and minimum error, 3.8%. For the background, we obtained: maximum error, 10.1%; mean error, 3.1%; and minimum error, <0.1%. It is worth noting that, in this case, only an approximate reconstruction can be obtained, as, for quite a complex object (like the two concentric spheres with different permittivity values), it is well-known that only a multiview process allows a correct shaping and an accurate quantitative permittivity imaging.

Multiview versions of the considered approach were proposed in the past for two-dimensional configurations [20], [27], [14]. These methods require that the electromagnetic source and the investigation and observation domains rotate jointly around the cross-section of an infinite cylinder in order to acquire multiview scattering data. In [14], the views are combined via a look-up table, and the improvement in the reconstruction (image contrast) is assessed. In addition, the use of a multiview approach seems to allow the reconstruction quality to be less sensitive to the number of independent columns. Of course, this should be shown for three-dimensional configurations. Unfortunately, as mentioned in the Introduction, a multiview approach for three-dimension al geometries is not yet available to the authors. So, considering the significance of this aspect, at least a two-dimensional example is provided. Let S be a square investigation area containing the unknown circular cross section of an infinite dielectric cylinder. This kind of scatterer is used to obtain input scattering data by means of analytical formulas [30]. We assume that: the square investigation area (side: $\lambda_o \times \lambda_o$) is partitioned into 64 square cells; the 65 measurement points are located (equally spaced) on an arc of a circumference of radius 11/15 λ_o; and the scatterer's dielectric permittivity is $\varepsilon_r = 3$. Using the look-up table to combine the views, the final reconstruction is obtained in the form of an 84 $\times$ 84-pixel image. Fig. 7 shows the contrast related to the reconstruction of the amplitude of the equivalent current density; such contrast can be defined as:

$$\mathrm{CONTR}\{\boldsymbol{K}\} = \frac{\xi(|\boldsymbol{K}|)_{\text{pixels inside the scatterer}}}{\xi(|\boldsymbol{K}|)_{\text{pixels outside the scatterer}}} \tag{8}$$

where the function $\xi(\tau)$ gives the mean value of τ. In particular, Fig. 7 gives the mean contrast values versus the number of independent columns, for 1, 8, 12 and 16 views. From this figure, one can first of all deduce that the single-view process allows a better reconstruction of the scatterer, whereas the multiview produces a certain spatial low-pass effect. On the other hand, the multiview process yields a far better reconstruction of the background, as pointed out in [14]. The second and more important aspect illustrated in Fig. 7 is the wide range of N_i values for which, when the multiview process is used, high contrast values can be obtained. For example, the mean contrast value is higher than 2.50 for $14 \leq N_i \leq 23$, for 8 views. This contrast value is reached by the single-view process only for $18 \leq N_i \leq 21$ and for $23 \leq N_i \leq 26$, but if one assumes $N_i = 22$, the maximum contrast value decreases to 1.70. As a consequence, for the multiview approach, the choice of a suitable number of independent columns is less critical, and the class of scatterers that can be reconstructed (once this number has been fixed) is much wider than for the single-view process.

As an additional example, we applied the multiview approach to an infinite cylinder made up of two cylinders whose circular cross-sections were not concentric. For this example, we assumed a square investigation area (side: $\lambda_o \times \lambda_o$), partitioned into 64 square cells; 16 measurement points were located (equally spaced) on three sides at a distance $\lambda_o/8$ from the investigation area. The two cylinders had the following permittivities and radii: $\varepsilon_r = 2$ and $a_1 = \lambda_o/8$ for the small cylinder, and $\varepsilon_r = 1.5$ and $a_2 = \lambda_o/2\sqrt{2}$ for the large one. If a coordinate system was placed in such a way that its center corresponded to the center of the investigation square (with the x and y axes parallel to the square edges), and an incident TM field (propagating in the x direction, with the $\boldsymbol{E}$-field polarized along the z axis) was used, the two circles (i.e., the cross-sections of the infinite cylinders) were centered at points $(\lambda_o/4, \lambda_o/4)$ and $(\lambda_o/4\sqrt{2}, \lambda_o/4\sqrt{2})$, respectively.

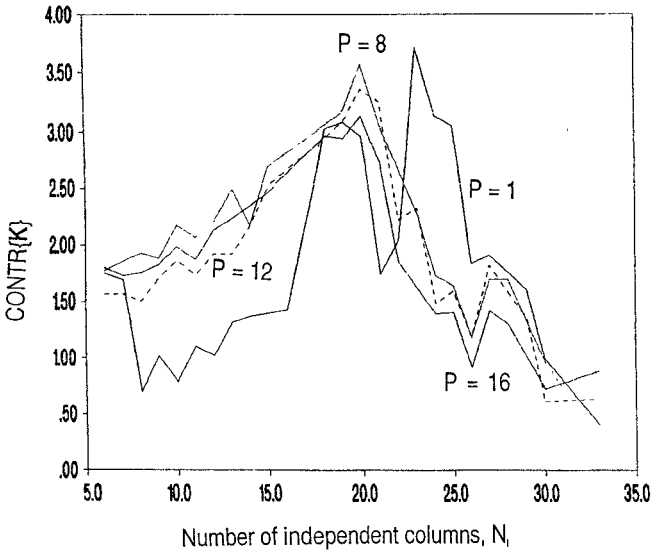

Fig. 7. Mean contrast values in the reconstruction of the amplitude of the equivalent current density (P: number of views).

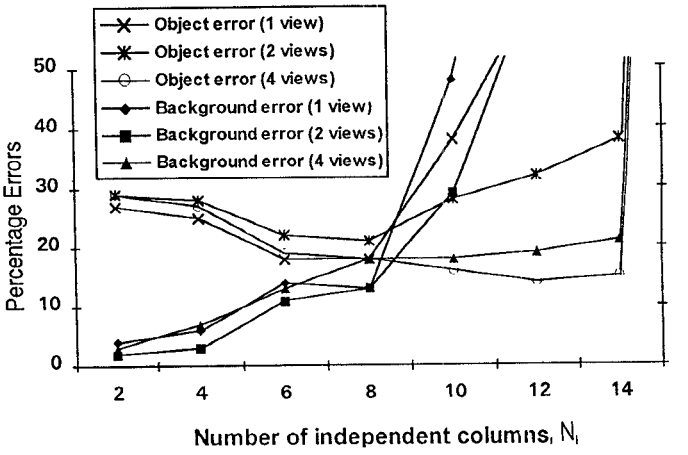

Fig. 8. Percentage errors on the reconstructions of the cross-sections of two nonconcentric dielectric infinite cylinders for different numbers of views.

Fig. 8 gives the percentage errors on the dielectric reconstructions of the object and of the background versus the number of independent columns, for 1, 2, and 4 views. In particular, the plotted values are the mean values of the percentage errors calculated for all the pixels inside (object reconstruction) and outside (background reconstruction) the cross-section of the scattering cylinder. As can be seen, the proposed criterion for the choice of the number of independent columns can be easily applied and, even though it does not guarantee the most desirable solution in all situations, it leads to an unequivocal choice of N_i . Most important, it appears evident that, in this case, too, the increase in the number of views can make the choice less critical. See, for example, in Fig. 8, the wide range of independent columns for which the percentage errors (both inside and outside the object) are below 20% for 4 views. In the other two cases (i.e., 1 and 2 views), errors less than 25% are obtained only for $6 \leq N_i \leq 8$.

IV. Modified Inversion Scheme and Results

In this section, we propose a modified inversion scheme that also increases the range from which to choose the number of independent columns that allows one to attain accurate dielectric reconstructions. With reference to Fig. 1, we can write the relationship between the total electric field and the equivalent current density inside the investigation domain V as

$$\boldsymbol{E}_{\text{tot}}(\boldsymbol{r}) = \boldsymbol{E}_{\text{inc}}(\boldsymbol{r}) + \int_V \boldsymbol{K}(\boldsymbol{r}') \cdot \Gamma_o(\boldsymbol{r}, \boldsymbol{r}') d\boldsymbol{r}' \qquad \boldsymbol{r} \in V. \quad (9)$$

Applying the MOM to (9), we obtain the relation

$$\Gamma'_{\text{NXN}} \underline{K}_{\text{NX1}} = \underline{E}'_{\text{tot,NX1}} - \underline{E}'_{\text{inc,NX1}}. \quad (10)$$

In our case, we can formally derive $\underline{K}_{\text{NX1}}$ in (10) and substitute it into (4). This procedure allows us to calculate directly the total electric field in the investigation domain by using the relation

$$\underline{E}_{\text{tot,MX1}} - \underline{E}_{\text{inc,MX1}} = \Gamma^{(2)}_{\text{MXN}} (\underline{E}'_{\text{tot,NX1}} - \underline{E}'_{\text{inc,NX1}}) \quad (11)$$

where $\Gamma^{(2)}_{\text{MXN}}$ is the product of matrix Γ_{MXN} multiplied by the inverse of Γ'_{NXN}. Matrix Γ'_{NXN} is a nonsingular square matrix, usually well-conditioned, which can be inverted directly by the Gauss algorithm. Solving system (11) allows us to calculate:

$$\underline{E}'_{\text{tot,NX1}} = \underline{E}'_{\text{inc,NX1}} + \Gamma^{(2)^*}_{\text{NXM}} (\underline{E}_{\text{tot,MX1}} - \underline{E}_{\text{inc,MX1}}) \quad (12)$$

where $\Gamma^{(2)^*}_{\text{NXM}}$ stands for the pseudoinverse matrix of matrix $\Gamma^{(2)}_{\text{MXN}}$. Once the total electric field inside the investigation domain is known, it is possible to calculate the distribution of the dielectric parameters in the same volume by using (12) and recalling (2) (in discretized form)

$$\underline{K}_{\text{NX1}} = V_{\text{NXN}} \underline{E}_{\text{tot,NX1}} \quad (13)$$

where V_{NXN} is a diagonal matrix whose elements are the coefficients of the series expansion of the unknown $V(\boldsymbol{r})$. Therefore, substituting (13) into (10), we obtain

$$\underline{E}_{\text{tot,NX1}} - \underline{E}_{\text{inc,NX1}} = \Gamma'_{\text{NXN}} V_{\text{NXN}} \underline{E}_{\text{tot,NX1}} \quad (14)$$

in which the scattering potential matrix, V_{NXN}, is the only unknown term, which can easily be derived, as the inverse matrix of matrix Γ'_{NXN} has already been calculated and stored. The new procedure does not require much more computations than the original one (the inverse of matrix Γ'_{NXN} can be performed off line), and would allow us to keep all the interesting features previously described if a multiview version were developed. The main advantage lies in the *inversion* of matrix $\Gamma^{(2)}_{\text{MXN}}$, which has proved to be less critical than the *inversion* of the Green matrix in the original procedure. It is worth noting that, in some applications, the knowledge of the internal electric field distribution may constitute the only objective of the investigation. In these cases, the last steps of the approach are not needed.

The new procedure does not require the calculation of the equivalent current density, hence we cannot apply the NSSC. In order to show the main advantages of the new method, we

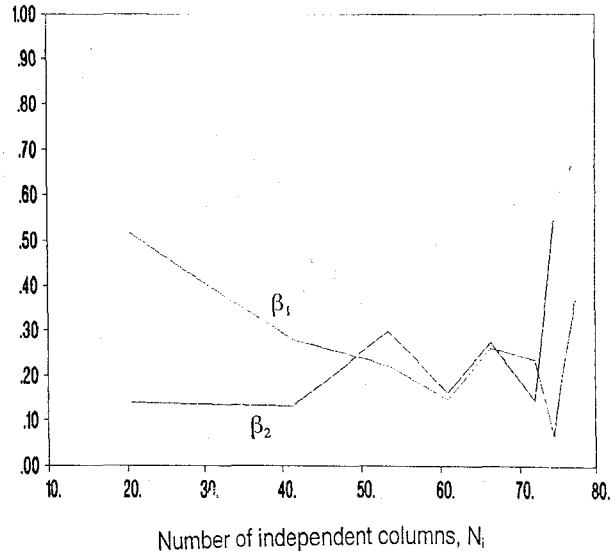

Fig. 9. Parameters β_1 and β_2 against the number of independent columns (N_i) (new procedure).

reconsider the same example of a 3D dielectric reconstruction as given in Section II. Fig. 9 gives the plots of the parameters β_1 and β_2 versus the number of independent columns. Two conclusions can be drawn from this figure. The first is that the proposed criterion (applied, in this case, on the basis of the reconstruction of the dielectric permittivity) leads to a nonunique choice of the number of independent columns ($N_i = 48; N_i = 68; N_i = 72$). However, the reconstruction results are quite similar for the three numbers, as can be deduced from the parameters β_1 and β_2, and as is confirmed by the results in Table II. This table gives the values of the reconstructed relative dielectric permittivities inside the 27 cells of the investigation volume for the N_i's given by the criterion and for some other different numbers of independent columns used for the purpose of comparison. The second and more important aspect is the existence of a range of N_i values (between 48 and 72) for which the behaviors of the parameters β_1 and β_2 are rather irregular, but the reconstruction quality is quite good (β_1 ranges between 0.16 and 0.27, and β_2 ranges between 0.16 and 0.30). As a consequence, when using the new procedure, the choice of the *optimal* number of independent columns is less critical, and a wider class of scatterers can be reconstructed for a fixed N_i value.

Finally, in order to evaluate the advantages of the new procedure for the reconstruction of the total internal electric field, we considered the dielectric reconstruction of a homogeneous object ($\varepsilon_R = 5$) that occupied four cells of the investigation domain. Fig. 10 gives the mean values of the percentage errors on the reconstruction of the total electric field inside the 27 cells of the investigation domain, for different values of the signal-to-noise ratio, S/N, related to the random noise added to the input data. As can be seen, for S/N = 80 dB, the new procedure yielded a worse reconstruction than the original procedure, due to the propagation errors incurred in the additional numerical computation. Instead, for S/N < 80 dB, the new procedure gave far better reconstructions (especially for lower S/N values). The obtained improvement

TABLE II
RECONSTRUCTED VALUES OF THE RELATIVE DIELECTRIC PERMITTIVITY INSIDE THE SCATTERER FOR SOME VALUES OF THE NUMBER OF INDEPENDENT COLUMNS (NEW PROCEDURE)

Cell number26	$N_i = 20$	$N_i = 41$	$N_i = 48$	$N_i = 68$	$N_i = 72$	$N_i = 77$
1	0.95	1.02	1.14	0.66	0.62	−0.32
2	1.42	.086	1.33	0.41	0.37	−0.07
3	0.93	1.03	1.37	0.63	0.48	−1.31
4	0.84	0.79	0.93	1.06	1.24	1.57
5	0.79	1.28	0.58	0.64	0.94	0.98
6	1.17	1.16	0.64	0.93	0.99	1.36
7	1.15	1.27	1.07	0.57	0.48	0.53
8	1.23	0.91	1.34	1.37	2.66	−0.53
9	0.87	0.97	1.10	0.63	0.60	0.61
10	1.12	1.38	1.12	0.90	0.98	1.04
11	1.24	0.96	1.38	0.71	0.18	1.96
12	0.99	0.75	0.98	2.63	1.62	1.84
13	1.10	0.71	0.76	0.51	0.60	−1.62
14	0.81	1.08	0.73	0.04	0.12	0.38
15	0.99	0.98	0.85	0.35	0.25	−0.80
16	0.98	1.16	0.90	1.25	1.89	0.87
17	1.12	0.89	1.37	1.15	−0.62	0.59
18	0.95	0.96	1.06	1.07	1.60	0.77
19	1.15	1.03	0.84	1.04	1.04	1.43
20	1.14	1.40	1.24	0.65	0.47	1.49
21	1.02	1.27	0.84	0.87	0.88	1.45
22	1.45	2.16	2.332	3.50	2.42	1.85
23	1.03	0.84	0.75	1.29	1.78	−0.43
24	0.93	0.88	1.89	1.37	1.62	1.29
25	0.95	0.71	0.68	1.08	1.10	0.80
26	1.14	0.98	1.03	0.99	0.84	0.04
27	0.82	1.06	0.50	1.01	0.97	0.73

is confirmed in Fig. 11, which shows the plot of the ratio between the values of the amplitude of the reconstructed total electric field and the values of the amplitude of the original total electric field inside the cells of the investigation domain. In this case, we assumed S/N = 40 dB. It is evident that a better reconstruction of the total electric field results in a better reconstruction of the scattering potential, as in the previous example. For completeness, Table III gives the percentage errors on the reconstructed phases of the total electric field. The table gives the minimun, mean and maximum phase errors inside the subdomains of the investigation area for different values of the S/N ratio and for the original and the new procedures.

V. CONCLUSION

In this paper, we have considered integral-equation-based numerical methods for microwave imaging that use regularization procedures to overcome ill-conditioning problems. In particular, approaches that employ the pseudoinversion algorithm have been assumed for illustration. The need for *a priori* information to obtain significant reconstruction results has been discussed, and the necessity (when numerical results are reported) for giving the values of the regularization parameters, or of other associated parameters (like the number of independent columns, if the pseudoinverse is used) has been proved. The use of a criterion for the choice of the number of independent columns has also been suggested, and a new criterion has been proposed and compared (where possible)

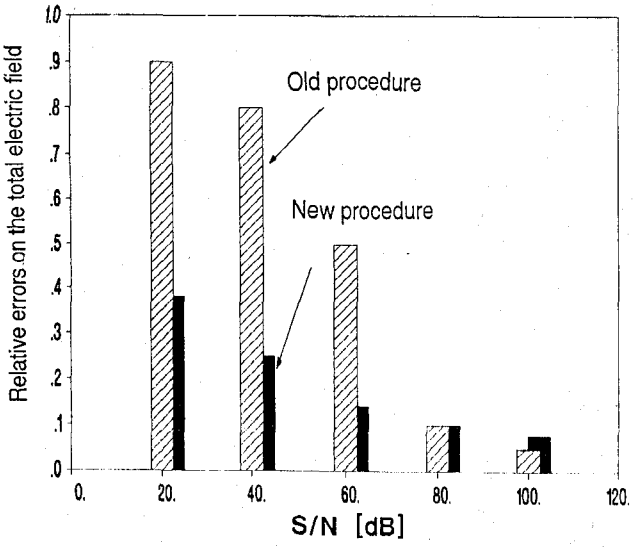

Fig. 10. Mean values of the relative errors on the reconstruction of the total electric field (amplitude) inside the investigation domain.

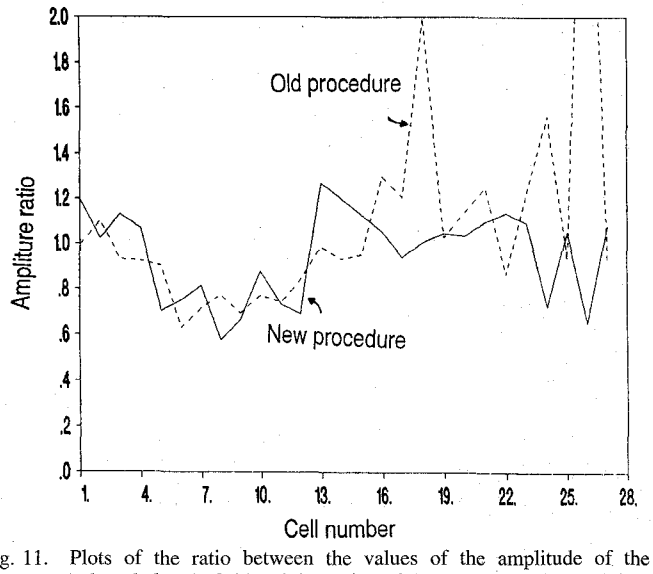

Fig. 11. Plots of the ratio between the values of the amplitude of the reconstructed total electric field and the values of the amplitude of the original total electric field.

TABLE III
PHASE ERRORS ON THE TOTAL ELECTRIC FIELD INSIDE THE SCATTERER FOR DIFFERENT VALUES OF THE S/N RATIO (ORIGINAL AND NEW PRODUCRUES)

	New procedure			Old procedure		
S/N↓	Minimum	Mean	Maximum	Minimum	Mean	Maximum
20	1.50	53.41	111.75	2.50	74.65	160.59
40	0.11	25.04	69.58	0.75	36.82	114.10
80	2.5 10^2	3.12	20.12	8.2 10^2	3.72	21.43
100	0.17	4.01	17.96	9.5 10^2	3.43	19.29

with the one suggested by Ney, Smith and Stuchly. Some approaches that allow a less critical choice of the number of independent columns have been discussed in order to extend the class of scatterers that can be successfully reconstructed for a given configuration. In particular, a multiview version of the moment-method numerical solution to the inverse-scattering problem has shown, in the case of two-dimensional imaging, a flatter plot of the reconstruction errors versus the number of independent columns than the plot related to the single-view process. As the whole paper refers to three-dimensional cases, it would be interesting to evaluate if the conclusions drawn for the two-dimensional approach may still hold true for multiview approaches to three-dimensional imaging. A 3D multiview version is currently under development. Finally, we have presented a new procedure that, without any significant increase in the computer resources required, improves the reconstruction process and allows one to choose from a wider range the number of independent columns to achieve accurate dielectric reconstructions. Such a procedure gives directly the values of the total internal electric field vector; this feature may be of interest in some applications. The capabilities of the new and the original procedures in computing the total internal electric field vector have been compared. Preliminary results indicate a notable improvement in the case of noisy input data.

REFERENCES

[1] E. Wolf, "Three-dimensional structure determination of semi-transparent objects from holographic data," *Optics Comm.*, vol. 1, no. 4, pp. 153–156, 1969.
[2] C. Pichot, L. Jofre, G. Peronnet, and J. C. Bolomey, "Active microwave imaging of inhomogeneous bodies," *IEEE Trans. Antennas Propagat.*, vol. AP-33, pp. 416–425, 1985.
[3] M. Slaney, A. C. Kak, and L. E. Larsen, "Limitation of imaging with first-order diffraction tomography," *IEEE Trans. Microwave Theory Tech.*, vol. MTT-32, pp. 860–873, 1984.
[4] J. C. Bolomey, C. Pichot, and G. Gaboriaud, "Planar microwave imaging camera for biomedical applications. Critical and prospective analysis of reconstruction algorithms," *Radio Sci.*, vol. 26, pp. 541–550, 1991.
[5] R. F. Harrington, *Field Computation by Moment Method.* New York: Macmillan, 1968.
[6] T. C. Guo and W. W. Guo, "Computation of electromagnetic wave scattering from an arbitrary three-dimensional inhomogeneous dielectric object," *IEEE Trans. Magn.*, vol. MAG-25, pp. 2872–2874, 1989.
[7] D. K. Ghodgaonkar, O. P. Gandhi, and M. J. Hagmann, "Estimation of complex permittivities of three-dimensional inhomogeneous biological bodies," *IEEE Trans. Microwave Theory Tech.*, vol. MTT-31, pp. 442–446, 1983.
[8] M. M. Ney, A. M. Smith, and S. S. Stuchly, "A solution of electromagnetic imaging using pseudoinverse transformation," *IEEE Trans. Med. Imag.*, vol. MI-3, pp. 155–162, 1984.
[9] S. Caorsi, G. L. Gragnani, and M. Pastorino, "Equivalent current density reconstruction for microwave imaging purposes," *IEEE Trans. Microwave Theory Tech.*, vol. MTT-37, no. 5, pp. 910–916, 1989.
[10] T. Sarkar, D. D. Weiner, and V. K. Jain, "Some mathematical considerations in dealing with the inverse problem," *IEEE Trans. Antennas Propagat.*, vol. AP-29, pp. 373–379, 1981.
[11] M. Z. Nashed, "Operator-theoretic and computational approach to ill-posed problems with applications to antenna theory," *IEEE Trans. Antennas Propagat.*, vol. AP-29, pp. 220–231, 1981.
[12] M. M. Ney, "Method of moments as applied to electromagnetic problems," *IEEE Trans. Microwave Theory Tech.*, vol. MTT-33, pp. 972–980, 1985.
[13] B. Rust, W. R. Burrus, and C. Schneeberger, "A simple algorithm for computing the generalized inverse of a matrix," *Commun. ACM*, vol. 9, pp. 381–387, 1966.
[14] S. Caorsi, G. L. Gragnani, and M. Pastorino, "An approach to microwave imaging using a multiview moment-method solution for a 2-D infinite cylinder," *IEEE Trans. Microwave Theory Tech.*, vol. MTT-39, pp. 1062–1067, 1990.
[15] C.-C. Chiu and Y.-W. Kiang, "Electromagnetic imaging for an imperfectly conducting cylinder," *IEEE Trans. Microwave Theory Tech.*, vol. MTT-39, pp. 1632–1639, 1991.
[16] F. X. Canning, "Singular-value decomposition of integral equations of EM and applications to the cavity resonance problem," *IEEE Trans. Antennas Propagat.*, vol. AP-37, pp. 1156–1163, 1989.
[17] W. W. Guo and T. C. Guo, "Dielectric imaging by microwave inverse scattering and a technique to stabilize matrix inversion," in *Proc. 2nd*

Int. Symp. on Recent Advances in Microwave Technol., Beijing, China, 1989, pp. 33–38.
[18] J. V. Candy and C. Pichot, "Active microwave imaging: A model-based approach," *IEEE Trans. Antennas Propagat.*, vol. AP-39, pp. 285–290, 1991.
[19] A. N. Tikhonov and V. Arsenine, *Solutions of Ill-Posed Problems.* New York: Winston, 1977.
[20] N. Joachimowicz, C. Pichot, and J.-P. Hugonin, "Inverse scattering: an iterative numerical method for electromagnetic imaging," *IEEE Trans. Antennas Propagat.*, vol. AP-39, pp. 1742–1752, 1991.
[21] T. Takanaka, H. Harada, and M. Tanaka, "On a simple diffraction tomography technique based on a modified Newton-Kantorovich method," *Microwave and Opt. Technol. Lett.*, vol. 5, pp. 94–97, 1992.
[22] A. J. Devaney, "Nonuniqueness in the inverse scattering problem," *J. Math. Phys.*, vol. 19, no. 7, pp. 1526–1691, 1978.
[23] W. R. Stone, "A review and examination of results on uniqueness in inverse problems," *Radio Sci.*, vol. 22, pp. 1026–1030, 1987.
[24] J. Van Bladel, *Electromagnetic Fields.* New York: McGraw Hill, 1964.
[25] C. T. Tai, *Dyadic Green's Functions in Electromagnetic Theory.* Scranton, PA: Intext Educational, 1971.
[26] S. Caorsi, G. L. Gragnani, and M. Pastorino, "Microwave imaging by three-dimensional Born linearization of electromagnetic scattering," *Radio Sci.*, vol. 25, pp. 1221–1229, 1990.
[27] M. J. Hagmann and R. L. Levine, "Procedures for noninvasive electromagnetic property and dosimetry measurements," *IEEE Trans. Antennas Propagat.*, vol. AP-38, pp. 99–106, 1990.
[28] S. Caorsi, G. L. Gragnani, and M. Pastorino, "Electromagnetic vision-oriented numerical solution to three-dimensional inverse scattering," *Radio Sci.*, vol. 23, pp. 1094–1106, 1988.
[29] J. A. Stratton, *Electromagnetic Theory.* New York: McGraw Hill, 1941.
[30] D. S. Jones, *The Theory of Electromagnetism.* Oxford: Pergamon, 1964.

Salvatore Caorsi received the "laurea" degree in electronic engineering from the University of Genoa, Genoa, Italy, in 1973.

After graduation he remained at the university as a researcher, and since 1976 he has been professor of antennas and propagation. In 1985 he also assumed the title of professor of Fundamentals of Remote Sensing. He is with the Department of Biophysical and Electronic Engineering, where he is responsible for the Applied Electromagnetics Group and for the Inter-university Research Center for Interactions Between Electromagnetic Fields and Biological Systems (ICEMB). His primary activities are focused on applications of electromagnetic fields to telecommunications, artificial vision and remote sensing, biology, and medicine. In particular, he is working on research projects concerning microwave hyperthermia and radiometry in oncological therapy, numerical methods for solving electromagnetic problems, and inverse scattering and microwave imaging.

Mr. Caorsi is a member of the Associazione Elettrotecnica ed Elettronica Italiana (AFI), of the European Bioelectromagnetism Association (EBEA) and of the European Society for Hyperthermic Oncology (ESHO).

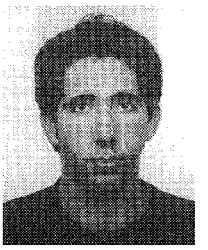

Stefano Ciaramella received the "laurea" degree in electronic engineering from the University of Genoa, Italy, in 1990. After graduation he collaborated with the activities of the Department of Biophysical and Electronic Engineering. His interests are in the fields of inverse scattering and microwave imaging.

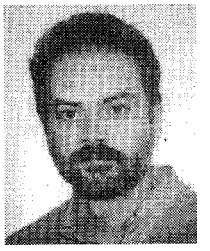

Gian Luigi Gragnani (M'89) received the "laurea" degree in electronic engineering from the University of Genoa, Genoa, Italy, in 1985.

In the same year, he joined the Applied Electromagnetics Group in the Department of Biophysical and Electronic Engineering (DIBE) and subsequently he has cooperated with the Inter-university Research Center for Interactions Between Electromagnetic Fields and Biological Systems. Since 1989 he has been responsible for the DIBE Applied Electromagnetics Laboratory. His primary research interests are in the field of electromagnetic scattering (both direct and inverse). In particular, he is engaded in doing research work on numerical methods for addressing electromagnetic problems, on microwave imaging, on biomedical applications of electromagnetic fields (especially microwave hyperthermia and radiometry), and on electromagnetic compatibility.

Mr. Gragnani is a member of the European Bioelectromagnetism Association (EBEA).

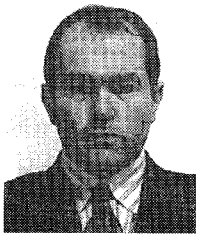

Matteo Pastorino (M'90) received the "laurea" degree in electronic engineering from the University of Genoa, Genoa, Italy, in 1987 and the Ph. D. degree in Electronics and Computer Science from the same university in 1992.

Since 1987, the year it was established, he has cooperated on the activities of the Applied Electromagnetics Group and on the activities of the Inter-university Research Center for Interactions Between Electromagnetic Fields and Biological Systems. He is an assistant professor of electromagnetic fields in the Department of Biophysical and Electronic Engineering. His main research interests are in electromagnetic direct and inverse scattering, microwave imaging, wave propagation in presence of nonlinear media, and in numerical methods in electromagnetism. He is also working on research projects concerning biomedical applications of e.m. fields and microwave hyperthermia.

Dr. Pastorino is a member of the Associazione Elettrotecnica ed Elettronica Italiana (AFI), and of the European Bioelectromagnetism Association (EBEA).